On the evolution of eddies in a rapidly rotating system

By P. A. DAVIDSON[1], P. J. STAPLEHURST[1] AND S. B. DALZIEL[2]

[1]Department of Engineering, University of Cambridge, Trumpington Street,
Cambridge CB2 1PZ, UK

[2]Department of Applied Mathematics and Theoretical Physics, University of Cambridge,
Wilberforce Rd, Cambridge CB3 0WA, UK

The formation of columnar eddies in a rapidly rotating environment is often attributed to nonlinear processes, acting on the nonlinear time scale $l/|\boldsymbol{u}|$. We argue that this is not the whole story, and that linear wave propagation can play an important role, at least on the short time scale of Ω^{-1}. In particular, we consider the initial value problem of a compact blob of vorticity (an eddy) sitting in a rapidly rotating environment. We show that, although the energy of the eddy disperses in all directions through inertial wave propagation, the axial components of its linear impulse and angular momentum disperse along the rotation axis only, remaining confined to the cylinder which circumscribes the initial vortex blob. This confinement has a crucial influence on the manner in which energy disperses from the eddy, with the energy density within the tangent cylinder remaining much higher than that outside (i.e. decaying as t^{-1} inside the cylinder and $t^{-3/2}$ outside). When the initial conditions consist of an array of vortex blobs the situation is more complicated, because the energy density within the tangent cylinder of any one blob is eventually swamped by the radiation released from all the other blobs. Nevertheless, we would expect that a turbulent flow which starts as a collection of blobs of vorticity will, for times of order Ω^{-1}, exhibit columnar vortices, albeit immersed in a random field of inertial waves. Laboratory experiments are described which do indeed show the emergence of columnar eddies through linear mechanisms, though these experiments are restricted to the case of inhomogeneous turbulence. Since the Rossby number in the experiments is of the order of unity, this suggests that linear effects can still influence and shape turbulence when nonlinear processes are also operating.

1. Introduction

We are interested in rapidly rotating turbulence in which the fluctuating velocity $|\boldsymbol{u}|$ is small, $|\boldsymbol{u}| \ll \Omega l$, where Ω is the bulk rate of rotation and l a suitable length scale. Such turbulence is known to be characterized by the growth of columnar eddies. Our primary concern is unforced, decaying turbulence in which the flow evolves from some specified initial state. Inertial waves play a central role in such flows, and indeed, when $\boldsymbol{u} \cdot \nabla \boldsymbol{u}$ is neglected by comparison with the Coriolis force, $2\boldsymbol{u} \times \boldsymbol{\Omega}$, the motion is just a spectrum of linear inertial waves. The frequency ϖ and group velocity $\boldsymbol{c}_g$ of these waves are dictated by the initial distribution of the wavevectors $\boldsymbol{k}$ according to (Greenspan 1968),

$$\varpi = \pm 2(\boldsymbol{\Omega} \cdot \boldsymbol{k})/|\boldsymbol{k}|, \quad \boldsymbol{c}_g = \pm 2\boldsymbol{k} \times (\boldsymbol{\Omega} \times \boldsymbol{k})/|\boldsymbol{k}|^3. \tag{1.1}$$

Since the initial distribution of k is often chosen to be random, it is by no means clear that there should be a preference for wave packets to propagate along the rotation axis, and thus there is no particular reason to expect columnar structures to form. Nevertheless, it seems that, under certain conditions, columnar eddies aligned with $\boldsymbol{\Omega}$ can indeed emerge (Hopfinger, Browand & Gagne 1982; Bartello, Metais & Lesieur 1994; Godeferd & Lollini 1999).

When $|\boldsymbol{u}| < \Omega l$, and t remains of order Ω^{-1}, it is natural to seek an explanation for this process in terms of linear wave theory, since $\boldsymbol{u} \cdot \nabla \boldsymbol{u}$ is small and there is no time for the cumulative effects of weak nonlinearity to influence the flow. However, many studies have suggested that anisotropy in the eddy structure emerges as a result of weak nonlinear interactions acting over the nonlinear time scale $l/|\boldsymbol{u}|$, as summarized in, for example, Cambon & Scott (1999) and Cambon (2001). Typically, these theories decompose the flow into a sea of inertial waves and investigate their near-resonant nonlinear interaction. The hypothesis is that, over the long time scale, $l/|\boldsymbol{u}|$, the near-resonant triad interactions can cause anisotropy, with a preferential transfer of energy into modes with horizontal wavevectors. There are two powerful arguments in favour of nonlinearity. First, when viscosity is neglected, the linearized equations are reversible, in the sense that they are unchanged under a reversal of $\boldsymbol{u}$. So for every initial condition which takes the eddy morphology from an isotropic state to an anisotropic one, say $\boldsymbol{u}^{(1)} \to \boldsymbol{u}^{(2)}$, we can find another initial condition which does the reverse, i.e. $-\boldsymbol{u}^{(2)} \to -\boldsymbol{u}^{(1)}$. Thus wave propagation cannot provide some universal, systematic mechanism for inducing anisotropy from arbitrary initial conditions. Of course, the nonlinear equations are also formally reversible in the inviscid limit, in the sense that they are unchanged under a reversal of $\boldsymbol{u}$, $\boldsymbol{\Omega}$ and t. However, the chaos associated with nonlinearity can, in effect, provide an arrow of time. The second argument in favour of nonlinearity is that, for homogeneous turbulence, the spectrum tensor Φ_{ij} shows no systematic tendency to develop anisotropy when $\boldsymbol{u} \cdot \nabla \boldsymbol{u}$ is suppressed. The proof of this is straightforward. In the linear regime, in which $\boldsymbol{u} \cdot \nabla \boldsymbol{u}$ is neglected by comparison with $2\boldsymbol{u} \times \boldsymbol{\Omega}$, we have

$$\partial^2 \hat{\boldsymbol{u}}/\partial t^2 + \varpi^2 \hat{\boldsymbol{u}} = 0, \qquad (1.2)$$

where $\hat{\boldsymbol{u}}$ is the Fourier transform (in space) of $\boldsymbol{u}$, ϖ is given by (1.1), and we have neglected viscosity. Let the initial distribution of $\hat{\boldsymbol{u}}(k)$ be $\hat{\boldsymbol{u}}^{(0)}(k)$. Noting that, in the linear regime, the vorticity equation $\partial \boldsymbol{\omega}/\partial t = 2\boldsymbol{\Omega} \cdot \nabla \boldsymbol{u}$ requires $\partial(\boldsymbol{k} \times \hat{\boldsymbol{u}}^{(0)})/\partial t = \varpi |\boldsymbol{k}| \hat{\boldsymbol{u}}^{(0)}$, (1.2) may be integrated to give

$$\hat{\boldsymbol{u}}(\boldsymbol{k}, t) = \hat{\boldsymbol{u}}^{(0)} \cos \varpi t - \left(\boldsymbol{k} \times \hat{\boldsymbol{u}}^{(0)}/k \right) \sin \varpi t. \qquad (1.3)$$

From this we can calculate Φ_{ij}, the Fourier transform of the two-point correlation $\langle u_i u_j' \rangle$:

$$2\Phi_{ij} = \Phi_{ij}^{(0)} + k^{-2} \varepsilon_{ipq} \varepsilon_{jmn} k_p k_m \Phi_{qn}^{(0)} + \left[\Phi_{ij}^{(0)} - k^{-2} \varepsilon_{ipq} \varepsilon_{jmn} k_p k_m \Phi_{qn}^{(0)} \right] \cos 2\varpi t$$
$$- k^{-1} \left[\varepsilon_{imn} k_m \Phi_{nj}^{(0)} + \varepsilon_{jpq} k_p \Phi_{iq}^{(0)} \right] \sin 2\varpi t. \qquad (1.4)$$

Equation (1.4) tells us that $\Phi_{ii} = \Phi_{ii}^{(0)}$, so that the energy spectrum, $E(k)$, cannot evolve in the linear regime. Moreover, in the particular case where $\Phi_{ij}^{(0)}$ is isotropic, we have the stronger condition $\Phi_{ij} = \Phi_{ij}^{(0)}$. So, for an inviscid fluid with isotropic initial conditions, anisotropy of Φ_{ij} cannot develop as a result of purely linearized dynamics. In fact it is possible to relax the assumption of isotropy. For example, for turbulence which is statistically axisymmetric about $\boldsymbol{\Omega} = \Omega \hat{\boldsymbol{e}}_z$, the tensor Φ_{ij} takes the form

$$\Phi_{ij} = (F + G)[k^2 \delta_{ij} - k_i k_j] - G \left[k_{\shortparallel}^2 \delta_{ij} + k^2 \lambda_i \lambda_j - k_{\shortparallel}(\lambda_i k_j + \lambda_j k_i) \right], \qquad (1.5)$$

where F and G are even functions of k and $k_{\shortparallel}$, and λ is a unit vector parallel to $\boldsymbol{\Omega}$. From (1.4) and (1.5) we see that

$$\Phi_{\shortparallel} = \Phi_{\shortparallel}^{(0)} + \frac{k_{\perp}^4}{2k^2} G^{(0)}[1 - \cos 2\varpi t], \quad \Phi_{\perp} = \Phi_{\perp}^{(0)} - \frac{k_{\perp}^4}{2k^2} G^{(0)}[1 - \cos 2\varpi t], \qquad (1.6)$$

where $\Phi_{\shortparallel} = \Phi_{zz}$, $\Phi_{\perp} = \Phi_{xx} + \Phi_{yy}$ and $G^{(0)}$ characterizes the initial anisotropy of the turbulence. For axisymmetric turbulence, then, the most that we can expect from linearized dynamics is an oscillation in $\Phi_{\perp}$ and $\Phi_{\shortparallel}$.

These arguments suggest that the appearance of columnar eddies in decaying, rotating turbulence is indeed a direct result of nonlinear interactions. However, since the study of third-order statistics by Gence & Frick (2001), it has been known that the second argument above is flawed, because these higher-order statistics *are* shaped by linear processes. The key reason why *second-order* (one-time) statistics are blind to the effects of linear waves is that all phase information is lost when we form an auto-correlation, and so all phase information is absent in the diagonal components of $\langle u_i u'_j \rangle$ and Φ_{ij}. (To recover phase information we must move to two-time, second-order statistics. See, for example, Cambon & Jacquin (1989).) Thus it is possible for a flow to evolve as a result of changes in the phases of the various Fourier modes, and this evolution will not be detected in the energy spectrum. Such changes in phase are precisely what occurs when energy is moved from place to place by linear wave propagation, i.e. energy redistribution by linear wave propagation is all about co-ordinating the phases of the various Fourier modes present, so that the location in space where the modes reinforce each other, rather than cancel, propagates with the group velocity (Lighthill 1978). In classical (non-rotating) turbulence, the phase information is essential to the emergence of coherent structures, and we contend that columnar eddies play a similar role in the rotating system.

This suggests that there is the possibility that, for certain classes of initial conditions, rapidly rotating flows evolve systematically on the fast time scale of Ω^{-1} as a result of linear inertial waves. Thus, just as linear processes are crucial in rapidly strained turbulence (cf. rapid distortion theory), so there is the possibility that linear waves can help shape rotating turbulence. Such a process cannot change isotropic turbulence into, say, two-dimensional turbulence, since Φ_{ij} is fixed by $\Phi_{ij}^{(0)}$, but it might allow distinctive coherent structures to develop. We now give an example of a class of initial conditions in which elongated structures emerge on the fast time scale through linear wave propagation, without the need for nonlinearity. We start by considering the evolution of a single, isolated eddy and then move to the case of turbulence emerging from a sea of randomly orientated vortex blobs.

2. The evolution of a single eddy at low Rossby number

2.1. *General concepts*

Consider an initial condition consisting of a compact blob of vorticity, $\boldsymbol{\omega}$, of arbitrary complexity sitting near the origin. Of course, for $t > 0$, energy will radiate away from the blob with a radiation pattern set by the initial distribution of wavevectors. In general, then, energy will disperse in all directions. However, we shall now show that this dispersion is (nearly) always biased towards the rotation axis. We start by noting that the linearized equation of motion for a homogeneous inviscid fluid demands that the angular momentum density, measured relative to an arbitrary origin, evolves according to

$$\partial(\boldsymbol{x} \times \boldsymbol{u})/\partial t = 2\boldsymbol{x} \times (\boldsymbol{u} \times \boldsymbol{\Omega}) + \nabla \times (p\boldsymbol{x}/\rho), \qquad (2.1)$$

whose axial component can be written in the form

$$\partial(\boldsymbol{x} \times \boldsymbol{u})_z/\partial t = -\nabla \cdot [(x^2 - z^2)\Omega\boldsymbol{u}] + [\nabla \times (p\boldsymbol{x}/\rho)]_z. \tag{2.2}$$

Let us integrate this over a cylindrical volume, centred on the z-axis, of radius R and infinite length. The pressure term drops out, because there is no net pressure torque acting on the cylinder, while the first term on the right-hand side integrates to zero because of continuity. It follows that the axial component of angular momentum, H_z, in such a cylinder is conserved, essentially because linear waves cannot support a net horizontal flux of axial angular momentum. Moreover, provided the cylinder encloses all of the vorticity initially present in the blob, H_z is equal to the angular impulse of the fluid:

$$H_z = \int_{V_R} (\boldsymbol{x} \times \boldsymbol{u})_z \, \mathrm{d}V = \frac{1}{3} \int_{V_\infty} (\boldsymbol{x} \times (\boldsymbol{x} \times \boldsymbol{\omega}))_z \, \mathrm{d}V. \tag{2.3}$$

(This follows from integrating the identity

$$6(\boldsymbol{x} \times \boldsymbol{u}) = 2\boldsymbol{x} \times (\boldsymbol{x} \times \boldsymbol{\omega}) + 3\nabla \times (x^2\boldsymbol{u}) - \boldsymbol{\omega} \cdot \nabla(x^2\boldsymbol{x}) \tag{2.4}$$

over the cylindrical volume V_R.) Consequently, at $t = 0$, the axial component of angular momentum is effectively contained within the cylinder which circumscribes the initial vortex blob, there being zero net angular momentum outside the cylinder. Since H_z is conserved within each annulus centred on the z-axis, it follows that the net axial component of angular momentum is confined for all time to the cylinder which circumscribes the initial vortex blob. Thus, while energy can disperse in all directions, the z-component of angular momentum can only disperse along the rotation axis.

Similarly, noting that the linearized vorticity equation, $\partial\boldsymbol{\omega}/\partial t = 2\boldsymbol{\Omega} \cdot \nabla\boldsymbol{u}$, may be rewritten in the form

$$\partial(\boldsymbol{x} \times \boldsymbol{\omega})/\partial t = 2(\boldsymbol{u} \times \boldsymbol{\Omega}) + 2\boldsymbol{\Omega} \cdot \nabla(\boldsymbol{x} \times \boldsymbol{u}), \tag{2.5}$$

and integrating this over the volume V_R, it may be shown that the axial component of linear impulse, $L_z = \frac{1}{2}\int(\boldsymbol{x} \times \boldsymbol{\omega})_z \, \mathrm{d}V$, is also confined to the cylinder which circumscribes the initial vortex blob. (We shall refer to this cylinder as the *tangent cylinder*.)

Now suppose that the initial vortex size is $\sim \delta$. Then the group velocity of the fastest inertial waves is of the order of $\sim \Omega\delta$ and so, after a time t, L_z and H_z become dispersed over a cylindrical region of radius δ and length $\sim \Omega\delta t$. Since, in this inviscid system, the axial components of the linear and angular impulse are conserved, the characteristic velocity on the axis can fall no faster than $|\boldsymbol{u}| \sim (\Omega t)^{-1}$. The energy of the eddy, on the other hand, disperses in all directions filling a volume of order $(\Omega\delta t)^3$ after time t. Since the total energy is also conserved, the typical velocity outside the tangent cylinder must fall at the faster rate of $|\boldsymbol{u}| \sim (\Omega t)^{-3/2}$. These two decay laws, $|\boldsymbol{u}| \sim (\Omega t)^{-1}$ and $|\boldsymbol{u}| \sim (\Omega t)^{-3/2}$, will be illustrated shortly by a simple, explicit example. In summary, then, the confinement of L_z and H_z to the tangent cylinder has a crucial influence on the manner in which energy disperses from an isolated eddy, with the energy density within the tangent cylinder remaining higher than that outside the cylinder.

2.2. A simple example

We can illustrate all of this by considering the trivial case of an eddy which has axial symmetry. When the flow is axisymmetric we can divide $\boldsymbol{u}$ into azimuthal and poloidal components. In (r, θ, z) coordinates we have

$$\boldsymbol{u} = (\Gamma/r)\hat{\boldsymbol{e}}_\theta + \nabla \times [(\psi/r)\hat{\boldsymbol{e}}_\theta], \tag{2.6}$$

where Γ is the angular momentum and ψ the Stokes streamfunction. The linearized inviscid vorticity equation then yields

$$\frac{\partial \Gamma}{\partial t} = 2\Omega \frac{\partial \psi}{\partial z}, \quad \frac{\partial}{\partial t}(r\omega_\theta) = 2\Omega \frac{\partial \Gamma}{\partial z}, \tag{2.7}$$

where $\nabla_*^2 \psi = (r\partial/\partial r)(r^{-1}\partial \psi/\partial r) + \partial^2 \psi/\partial z^2 = -r\omega_\theta$, ∇_*^2 being the Stokes operator. These may be combined to give the wave-like equation

$$\frac{\partial^2}{\partial t^2}\nabla_*^2 \Gamma + (2\Omega)^2 \frac{\partial^2 \Gamma}{\partial z^2} = 0. \tag{2.8}$$

This is most readily solved by introducing the Hankel-cosine transform

$$\hat{u}_\theta = \frac{1}{2\pi^2}\int_0^\infty \int_0^\infty r u_\theta J_1(k_r r) \cos(k_z z) \, \mathrm{d}r \, \mathrm{d}z, \tag{2.9}$$

where J_1 is the usual Bessel function (Davidson 1997). Adopting the initial conditions $\hat{u}_\theta = \hat{u}_\theta^{(0)}$ and $\psi = 0$, we find $\hat{u}_\theta = \hat{u}_\theta^{(0)} \cos \varpi t$, from which

$$u_\theta = 2\pi \int_0^\infty \int_0^\infty k_r \hat{u}_\theta^{(0)} J_1(k_r r) [\cos(k_z(z - 2\Omega t/k)) + \cos(k_z(z + 2\Omega t/k))] \, \mathrm{d}k_r \, \mathrm{d}k_z. \tag{2.10}$$

We now choose a simple initial condition for u_θ in the form of a Gaussian eddy:

$$u_\theta^{(0)} = \Lambda r \exp[-(r^2 + z^2)/\delta^2], \tag{2.11}$$

where δ is the characteristic eddy size and Λ an angular velocity. Equation (2.10) then yields

$$u_\theta = \frac{\Lambda \delta^5}{8\pi^{1/2}}\int_0^\infty k_r^2 \exp[-k_r^2 \delta^2/4] J_1(k_r r) I(k_r) \, \mathrm{d}k_r, \tag{2.12}$$

where

$$I(k_r) = \int_0^\infty \exp\left[-k_z^2 \delta^2/4\right][\cos(k_z(z - 2\Omega t/k)) + \cos(k_z(z + 2\Omega t/k))] \, \mathrm{d}k_z. \tag{2.13}$$

Integrals (2.12) and (2.13) can be evaluated numerically and a typical snapshot of the flow, at $2\Omega t = 20$, is shown in figure 1(a) for $z > 0$. Although energy disperses in all directions, the energy density is clearly highest near the rotation axis, as anticipated above. The main characteristics of the solution (2.12), (2.13) may be exposed using a simple approximation. It is readily confirmed that, for this simple Gaussian eddy, the power spectrum for $\hat{u}_\theta^{(0)}$ is dominated by wavevectors in the vicinity of $k_z \approx 0$, $k_r \sim \delta^{-1}$. So a reasonable approximation to integral (2.13) is obtained by putting $k_z/k \approx k_z/k_r$ in the argument of the cosines. The integral I can then be evaluated exactly and we find

$$u_\theta \approx \Lambda \delta \int_0^\infty \kappa^2 \mathrm{e}^{-\kappa^2} J_1(2\kappa r/\delta) \left[\exp\left[-\left(\frac{z}{\delta} - \frac{\Omega t}{\kappa}\right)^2\right] + \exp\left[-\left(\frac{z}{\delta} + \frac{\Omega t}{\kappa}\right)^2\right]\right] \mathrm{d}\kappa, \tag{2.14}$$

where $\kappa = k_r \delta/2$. This approximation to the flow is shown in figure 1(b) for $2\Omega t = 20$. Although (2.14) somewhat underestimates the radial dispersion of energy, because it is biased towards horizontal wavevectors, it captures reasonably accurately the evolution of the primary structure near the axis.

Equation (2.14) has the advantage over (2.12) and (2.13) in that it is particularly easy to interpret. It tells us that kinetic energy disperses primarily in the $\pm z$-directions with the energy corresponding to wavenumber k_r located in the vicinity
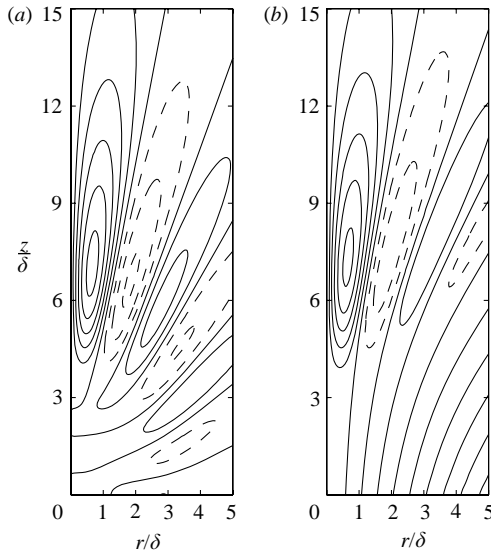
FIGURE 1. The evolution of an initially spherical vortex into a pair of columnar eddies by linear wave propagation. (*a*) The exact solution (2.12), (2.13) at $2\Omega t = 20$. (*b*) The approximate solution (2.14) at $2\Omega t = 20$. Dotted lines represent negative swirl.

of $z \sim \pm 2\Omega t / k_r = \pm \delta \Omega t / \kappa$. Note that the integral is dominated by contributions in which $\kappa \sim 1$, and that the energy corresponding to $\kappa = 1$ finds itself located near $z \sim \pm \delta \Omega t$. Thus kinetic energy disperses along the z-axis, forming two columnar structures with centres located at $z \sim \pm \delta \Omega t$ and length scales which grow as $l_z \sim \delta \Omega t$. Of course, this is precisely what we would expect from a simple group velocity argument based on (1.1).

The precise form of (2.14) at large times is readily found by insisting that the arguments in the exponential functions remain of order unity as $\Omega t \to \infty$. Consider the location $z = \delta \Omega t$. Then the only contribution to (2.14) comes from the wavevectors $\kappa = 1 \pm O((\Omega t)^{-1})$, and so (2.14) integrates to give

$$u_\theta(r, z = \delta \Omega t) \approx \Lambda \delta \sqrt{\pi/e^2} J_1(2r/\delta)(\Omega t)^{-1}, \quad \Omega t \to \infty. \quad (2.15)$$

Within the tangent cylinder, $r < \delta$, this yields $u_\theta \sim \Lambda \delta (\Omega t)^{-1}$, as anticipated above. Well outside the tangent cylinder, on the other hand, we find $u_\theta \sim \Lambda \delta (\Omega t)^{-3/2}(r/z)^{-1/2}$, which is also in line with our earlier discussion. Precisely the same results may be obtained from the exact solution (2.12), (2.13).

In summary, then, energy radiates in all directions, but the kinetic energy density is highest within the tangent cylinder where it disperses to form two columnar clouds with centres located at $z \sim \pm \delta \Omega t$ and axial length scales which grow as $l_z \sim \delta \Omega t$. Moreover this behaviour is expected to be common to any initial condition in which the vorticity is localized in space. (We shall ignore degenerate cases in which L_z and H_z are both zero.) Note, however, that the percentage of total energy contained within the tangent cylinder falls as $(\Omega t)^{-1}$, so that eventually the columnar structure becomes very weak, although the energy density will remain higher than that outside the cylinder. Note also that this transformation in eddy morphology occurs without any change in the power spectrum of $\hat{u}$, since it is accomplished simply by coordinated changes in phase.

3. The evolution of multiple eddies at low Rossby number

Let us now move from a single eddy to a distributed field of vorticity. (We continue to take $Ro \ll 1$ and Ωt of the order of unity.) Here the initial conditions are crucial. For example, if we start from a sea of discrete, randomly shaped vortex blobs then each one will disperse in the manner outlined above. Energy will radiate from the blobs forming a sea of random waves, yet embedded within this field of waves we would expect to see columnar structures emerge from the initial vortex cores. However, these columnar eddies will eventually be swamped by the random radiation because the percentage of energy within them falls as $(\Omega t)^{-1}$, whereas the energy within the cylinder that has radiated from all the other blobs will increase to a constant that is related to the volume fraction containing the initial eddies. Nevertheless, the columnar vortices should be evident for several rotation periods, provided that the eddies are not too closely packed. (If the eddies are closely packed, however, and the initial conditions are homogeneous, it is likely that any would-be column will rapidly fall prey to the random radiation.)

On the other hand, if we start with random Fourier modes without any phase coherence, we will see no columnar structures emerge on the linear time scale, simply because there are no blobs to initiate the columns. In other words, the formation of columnar structures in the examples above is achieved through a careful rearrangement of the relative phases of the Fourier modes, and if there is no phase coherence at $t = 0$ this process cannot occur. The latter initial condition is often (but by no means always) favoured by those performing numerical experiments, while the former would be more typical of a laboratory experiment in which the fluid is stirred up and then left. (Think of the Kármán vortices shed immediately behind a grid in conventional grid turbulence.) We shall describe just such an experiment in § 5.

4. Speculation about turbulence at Rossby number order unity

So far we have assumed that $|\boldsymbol{u}| \ll \Omega l$, so that inertia could be ignored by comparison with the Coriolis force, at least on the time scale of Ω^{-1}. However, let us now speculate about what happens when we allow for a finite, though modest, amount of inertia. We shall assume that the Rossby number, $Ro = |\boldsymbol{u}|/2\Omega l$, is not too large, so that inertial waves still operate, yet not too small, so that the linear and nonlinear time scales are not too disparate. Then the formation of columnar structures on the linear time scale, Ω^{-1}, could, in turn, provide a catalyst for nonlinear interactions since these elongated vortices will tend to interact nonlinearly with the surrounding vorticity field. This would require the nonlinear time scale, $l/|\boldsymbol{u}|$, to be close to Ω^{-1}, so that a significant amount of nonlinear interaction could occur before the columnar eddies die out. If such a situation did arise we would expect to see the integral scale l_z, defined, say, in terms of the integral of the auto-correlation $\langle u_x(\boldsymbol{x}) u'_x(\boldsymbol{x} + z\hat{\boldsymbol{e}}_z) \rangle$, to exhibit a linear growth in time, shadowing the linear growth in the columnar vortices. (By contrast, l grows as $t^{2/7}$ in isotropic turbulence.) Interestingly, there is clear evidence of a linear growth of l_z for $Ro \sim 1$ in the rotating grid turbulence experiments of Jacquin *et al.* (1990).

There is a second mechanism by which linear and nonlinear dynamics could interact when $Ro \sim 1$. Nonlinearity continually reorganizes the vorticity field via vortex stretching. This rearrangement of the vorticity thus creates a continual sequence of new initial conditions on which the linear dynamics can operate. If the nonlinear dynamics tend to favour the formation of coherent vortical structures, then the arguments of
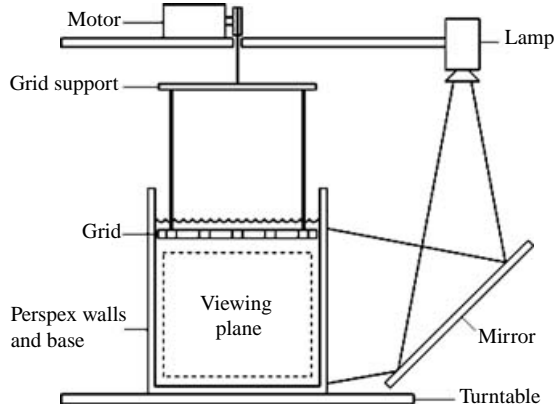
FIGURE 2. The apparatus.

§2 suggest that inertial waves will systematically elongate those structures along the rotation axis. Whether or not this does indeed occur requires further investigation.

5. An experiment at Rossby number of order unity

To illustrate these theoretical ideas we have performed a variant of the experiments of Dickinson & Long (1983) and Morize, Moisy & Rabaud (2005). Dickinson & Long created a cloud of turbulence in a rotating tank by continuously oscillating a grid. The turbulence initially occupies only a small part of the tank, but then spreads in the vertical direction. They observed that, when the rotation is weak, the turbulent cloud spreads axially at a rate $L_z \sim t^{1/2}$, but when rotation is dominant, it spreads at the faster rate $L_z \sim t$. They attributed the weak rotation result to conventional turbulent diffusion, and the linear growth for strong rotation to inertial waves. We have repeated their experiment except that, instead of continually oscillating the grid, we oscillate just once in the vertical direction, creating an initial cloud of turbulence which is then free to evolve. The tank was 45 cm square by 60 cm deep, filled with water to a depth of 50 cm (figure 2). We used two grids, with mesh sizes, M, of 5 cm and 8 cm, 64% porosity, and a bar width, $b = M/5$. The amplitude of the initial oscillation was ~ 10 cm, which defines the vertical extent of the initial turbulent cloud, and the average speed of the mesh was 10 cm s^{-1}. Experiments were carried out at rotation rates of $\Omega = 1$, 1.5 and 2 rad s^{-1}, and the turbulence visualized using Pearlescence which highlights regions of strong shear (Savaş 1985). The initial Rossby number, $|\boldsymbol{u}|/2\Omega b$, based on the bar width and the root-mean-square velocity of the fluid, lies in the range 1.5–3.5. The flow was illuminated with a vertical light sheet and images of reflected light intensity captured by camera.

Figure 3 shows typical images taken a few rotation periods after initiation of the turbulence, at $2\Omega t = 20$ (figure 3*a*) and 60 (figure 3*b*), by which time the turbulence fills the tank. The mesh size was $M = 8$ cm and the rotation rate 2 rad s^{-1}. At $2\Omega t = 20$, the turbulent cloud has 'a streaky' appearance characterized by elongated columnar structures, individually reminiscent of the structure seen in figure 1.

We have tracked the evolution of these columnar structures in a sequence of experiments for all three rotation rates and for both mesh sizes. The location of the leading edge of the structures was determined by eye to an accuracy of better than ± 5 mm. It is clear that we see the evolution of identifiable columnar structures rather
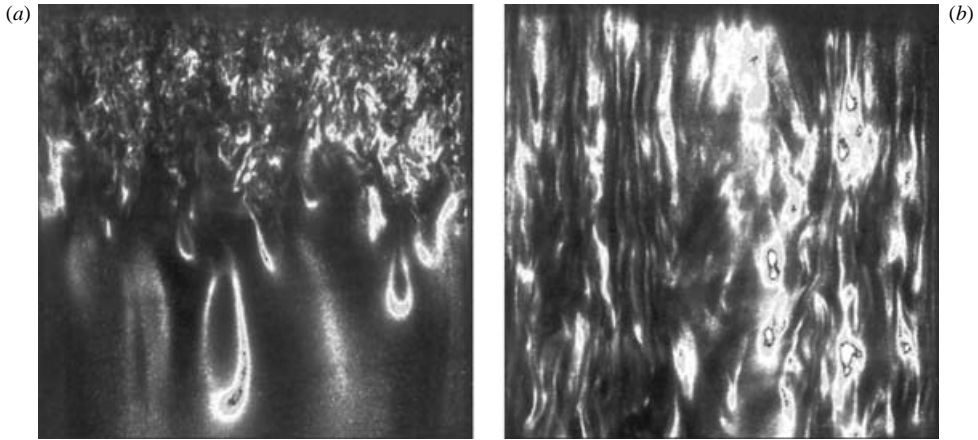
FIGURE 3. Images of the flow taken at different times after initiation of the turbulence. (*a*) $2\Omega t = 20$, (*b*) $2\Omega t = 60$. The mesh size was $M = 8\,\text{cm}$ and the rotation rate $2\,\text{rad s}^{-1}$. Note that columnar vortices are still evident at $2\Omega t = 60$. The images are $42\,\text{cm}$ square.
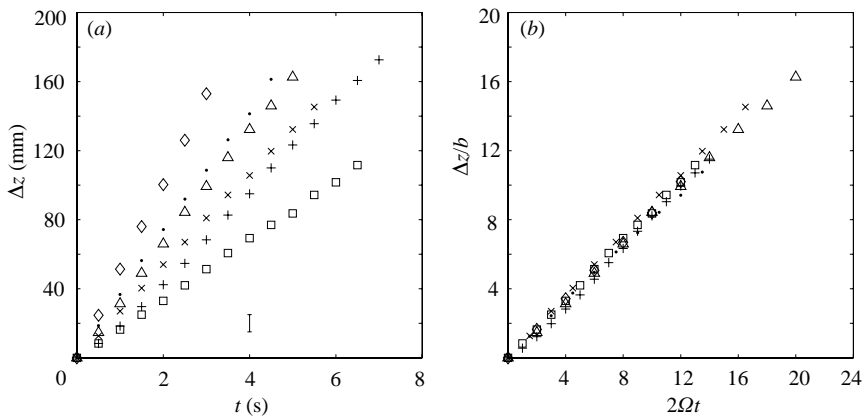

FIGURE 4. The distance travelled by the leading edge of typical columnar structures as a function of time. In (*b*) Δz and t are normalized by bar size, b, and Ω^{-1}, respectively. $\diamond$ ($M = 8\,\text{cm}$, $\Omega = 2\,\text{rad s}^{-1}$), $\bullet$ ($M = 8\,\text{cm}$, $\Omega = 1.5\,\text{rad s}^{-1}$), $+$ ($M = 8\,\text{cm}$, $\Omega = 1\,\text{rad s}^{-1}$), $\triangle$ ($M = 5\,\text{cm}$, $\Omega = 2\,\text{rad s}^{-1}$), $\times$ ($M = 5\,\text{cm}$, $\Omega = 1.5\,\text{rad s}$), $\square$ ($M = 5\,\text{cm}$, $\Omega = 1\,\text{rad s}^{-1}$).

than the random superposition of inertial waves from the turbulent cloud. Individual structures maintain their morphology from one frame to the next and propagate vertically downwards in a manner similar to that seen in §2. Structures with a larger horizontal length scale emerge first from the initial cloud of turbulence and propagate downwards more quickly than the smaller structures that emerge later.

Figure 4(*a*) shows the distance travelled, Δz, by the leading edge of the columnar structures as a function of time, each set of data being an ensemble of three nominally identical experiments. The growth in each case is clearly linear, consistent with linear wave propagation and the results of Dickinson & Long (1983). To confirm that these are indeed inertial waves, figure 4(*b*) shows the same data but with distance normalized by bar size and time normalized by rotation rate. According to expression (1.1) for the group velocity of inertial waves, such a normalization should collapse

the data from all of the experiments, and indeed it does. There is no doubt, therefore, that these columnar structures are the manifestation of linear inertial waves.

Turning now to the image in figure 3(*b*) we see that, at $2\Omega t = 60$, columnar vortices are evident, though immersed in a sea of turbulence. Since $Ro \sim 1$ we expect that both linear (wave-like) and nonlinear (vortex stretching) processes are occurring here. This suggests, but does not prove, that linear mechanisms continue to shape the turbulence even in the presence of nonlinear dynamics.

6. Conclusions

The short-term evolution of an inhomogeneous cloud of rotating turbulence, and the surrounding flow, is dominated by the growth of columnar structures, and these grow by inertial wave propagation in accordance with linear theory. The significance of this for homogeneous turbulence, or for turbulence evolving for times much longer than the rotation period, remains unclear. We may anticipate, however, that linear mechanisms will be more important when the initial conditions are characterized by coherent structures than by a structureless sea of vorticity. The distinction between coherent structures and a random sea is embodied in the phase information which we traditionally discard when characterizing turbulence in terms of spectral quantities.

REFERENCES

BARTELLO, P., METAIS, O. & LESIEUR, M. 1994 Coherent structures in rotating three-dimensional turbulence. *J. Fluid Mech.* **237**, 1–29.

CAMBON, C. 2001 Turbulence and vortex structures in rotating stratified flows. *Eur. J. Mech.* B *Fluids* **20**, 489–510.

CAMBON, C. & JACQUIN, L. 1989 Spectral approach to non-isotropic turbulence subjected to rotation. *J. Fluid Mech.* **202**, 295–317.

CAMBON, C. & SCOTT, J. F. 1999 Linear and nonlinear models of anisotropic turbulence. *Annu. Rev. Fluid Mech.* **31**, 1–45.

DAVIDSON, P. A. 1997 The role of angular momentum in the magnetic damping of turbulence. *J. Fluid Mech.* **336**, 123–150.

DICKINSON, S. C. & LONG, R. R. 1983 Oscillating-grid turbulence including effects of rotation. *J. Fluid Mech.* **126**, 315–333.

GENCE, J.-N. & FRICK, C. 2001 Naissance des correlations triple de vorticite dans une turbulence homogene soumise a une rotation. *C. R. Acad. Sci. Paris* II **329**, 351–356.

GODEFERD, F. S. & LOLLINI, L. 1999 Direct numerical simulation of turbulence with confinement and rotation. *J. Fluid Mech.* **393**, 257–308.

GREENSPAN, H. P. 1968 *Theory of Rotating Fluids*. Cambridge University Press.

HOPFINGER, E. J., BROWAND, F. K. & GAGNE, Y. 1982 Turbulence and waves in a rotating tank. *J. Fluid Mech.* **125**, 505–534.

JACQUIN, L., LEUCHTER, O., CAMBON, C. & MATHIEU, J. 1990 Homogeneous turbulence in the presence of rotation. *J. Fluid Mech.* **220**, 1–52.

LIGHTHILL, J. 1978 *Waves in Fluids*. Cambridge University Press.

MORIZE, C., MOISY, F. & RABAUD, M. 2005 Decaying grid-generated turbulence in a rotating tank. *Phys. Fluids* **17**, 095105.

SAVAŞ, O. 1985 On flow visualisation using reflective flakes. *J. Fluid Mech.* **152**, 235–248.